YTUP

Journal of Thermal Engineering

https://jten.yildiz.edu.tr/

https://doi.org/10.47481/jten.0044

RESEARCH ARTICLE

Comprehensive analysis of unsteady nanofluid flow with spatially varying concentration and imposed thermal flux over an impulsively initiated vertical plate

Nirmala M.[1,2], E.Geetha[1,*], S.Sarala[3], G.Sumathi[4], M.Mageswari[5], M.Radha Madhavi[6]

[1]Department of Mathematics, Sri Chandrasekharendra Saraswathi Viswa Maha Vidyalaya, Enathur, Kanchipuram, 603202, Tamil Nadu, India
[2]Department of Mathematics, Kumararani Meena Muthiah College of Arts and Science, Adyar, Chennai. 600020, Tamil Nadu, India
[3]Department of Mathematics, Kongunadu College of Engineering and Technology (Autonomous), Trichy, 621215, Tamil Nadu, India
[4]Department of Mathematics and Actuarial Science, B.S Abdur Rahman Crescent Institute of Science and Technology. Vandalur, Chennai, 600048, Tamil Nadu, India
[5]Department of Mathematics, Thanthai Periyar Government Institute of Technology, Vellore, 632002, India
[6]Department of Engineering Mathematics, College of Engineering, Koneru Lakshmaiah Education Foundation, Vaddeswaram, Andhra Pradesh, 522502, India

Abstract

This study investigates a critical problem: unsteady nanofluid flow with spatially varying particle concentration over impulsively started vertical plates subjected to imposed thermal flux, addressing a significant gap in understanding transient heat transfer mechanisms essential for optimizing thermal management systems. The research employs the Buongiorno two-phase model incorporating Brownian motion and thermal flux, with the governing equations solved analytically using the Laplace transform technique under realistic initial and boundary conditions. Key quantitative findings reveal that increasing the Brownian motion parameter from 0.1 to 0.5 enhances thermal conductivity by 15-25%, thickening the concentration boundary layer by 40-60%. Copper nanofluid exhibits 18-32% higher heat transfer rates than the base fluid, with optimal performance at a nanoparticle volume fraction of 2-4%. Higher thermal Grashof numbers (10^5-10^6) increase fluid velocity by 25-40% and reduce near-wall nanoparticle concentrations by 20-30%. The novelty lies in the comprehensive analysis of coupled transient momentum, energy, and species transport with spatially dependent thermophysical properties, extending beyond previous steady-state or uniform concentration studies. These findings provide quantitative design guidelines for nanofluid-based thermal systems, demonstrating that controlled nanoparticle distribution and transient thermal loading can significantly enhance heat transfer performance in industrial applications. The study shows that Brownian motion and heat flux markedly enhance heat and mass transport, leading to improved thermal performance. Copper-based nanofluids achieve significantly higher heat transfer rates than the base fluid, with optimal efficiency at moderate nanoparticle concentrations. Increased thermal buoyancy further accelerates fluid motion while limiting nanoparticle accumulation near the surface.

Keywords: Copper nanofluid, thermal flux, variable concentration, impulsive movement, vertical plate

Cite this article as: Nirmala, M., Geetha, E., Sarala, S., Sumathi, G., Mageswari, M., & Radha Madhavi, M. (2026). Comprehensive analysis of unsteady nanofluid flow with spatially varying concentration and imposed thermal flux over an impulsively initiated vertical plate. Journal of Thermal Engineering, 12(4), 1466–1479. https://doi.org/10.47481/jten.0044

1. Introduction

Engineered fluids represent a class of specially formulated substances designed with enhanced physical, chemical, and thermal properties for specific applications. These fluids are developed by systematically incorporating additives, such as polymers, surfactants, and nanoparticles, into conventional base fluids. Among the most promising developments in this field are nanofluids, which utilize nanoparticles composed primarily of metals, metal oxides, and carbon materials. The applications of nanofluids span diverse sectors, including nuclear reactors, electronic cooling systems, automotive industries, and medical diagnostics. Copper nanoparticle-enhanced fluids exemplify this technology; they consist of nanoscale cop-

*Corresponding Author
E-mail Adress: geethamuthu06@gmail.com

Submitted: 22 July 2025; **Accepted:** 17 January 2025

This paper was recommended for publication in revised form by Editor-in-Chief Ahmet Selim Dalkılıç

per particles suspended in media such as water, ethylene glycol, or lubricants to achieve superior thermal conductivity and heat-transfer performance.

In this study, spherical copper (Cu) nanoparticles with diameters ranging from 20 to 50 nm were dispersed in water as the base fluid due to copper's exceptional thermal conductivity (401 W/m·K) and superior heat-transfer enhancement capabilities. The Cu-water nanofluid system is selected for its proven thermal performance, with copper nanoparticles exhibiting a high density (8933 kg/m^3) and thermal stability in aqueous solutions. This combination ensures optimal Brownian-motion effects and reliable thermophysical property correlations, which are essential for accurate numerical modeling of the unsteady flow and heat-transfer phenomena.

The impulsively started vertical plate problem represents a fundamental case study in fluid mechanics, where a stationary flat plate immersed in viscous fluid suddenly begins moving at constant velocity parallel to its surface. This canonical problem serves as a benchmark for investigating unsteady boundary layer formation and transient viscous effects in incompressible Newtonian fluids. Understanding the influence of dimensionless parameters on thermal and mass transfer processes is crucial for optimizing system performance and advancing engineering solutions.

Astick Banerjee et al. [1] examined separation control and boundary-layer development of a Newtonian fluid flowing through a diverging permeable channel filled with a Darcy–Forchheimer porous medium under the influence of suction and injection. The analysis shows that when the sum of the Darcy permeability parameter and twice the Forchheimer parameter exceeds two, a boundary layer persists for all levels of mass suction or injection, and even in the absence of wall mass transfer.

Chandra Reddy et al. [2] conducted a comprehensive investigation of free convective magnetohydrodynamic nanofluid flow past moving vertical plates under simultaneous radiation and thermal diffusion effects. Their study revealed the complex interplay between magnetic forces, thermal radiation, and Soret effects, demonstrating how these combined phenomena influence velocity and temperature distributions in nanofluid boundary layers. The research highlighted the importance of thermal diffusion in mass transfer processes, particularly in applications where concentration gradients play critical roles in system performance. Building upon this foundation, Chandrakala et al. [3] investigated magnetohydrodynamic (MHD) effects on impulsively started vertical plate flows. Their findings demonstrated a reduction in velocity under the influence of a magnetic field and revealed contrasting effects of generative and destructive chemical reactions on hydrodynamic and concentration fields.

Djebali et al. [4] studied a simplified formulation for the similarity solution of boundary-layer flow developing along a vertically heated flat plate under buoyancy effects. A new analytical formulation is derived, and, using a Taylor series expansion approach, the classical case of an isothermal, infinite vertical flat plate is examined. The results show excellent agreement with both the fifth-order Runge–Kutta–Fehlberg (RKF45) numerical solutions and available experimental data. However, the boundary-layer behaviour along the vertical isothermal walls of a differentially heated cavity cannot be treated as a segment of an infinite hot or cold plate, owing to the transverse inflow of colder fluid and the intrusion of fluid beneath the cavity ceiling.

Duguma et al. [5] explored the flow and heat transfer characteristics of copper-water Casson nanofluid over a stretching or shrinking surface with slip conditions embedded within a porous medium. Their research identified multiple solution branches of the governing equations and performed a stability analysis to determine which solutions were physically realizable under various parametric conditions. The investigation provided insights into non-Newtonian nanofluid behavior in porous environments, which are significant for applications in materials processing and thermal engineering systems involving deformable boundaries. Hayat et al. [6] investigated three-dimensional rotating flows of Ag-CuO/water hybrid nanofluids, incorporating thermal radiation, heat generation and chemical reactions over linearly stretching surfaces. Their findings confirmed that hybrid nanofluids enhance temperature distribution and increase heat transfer rates on surfaces. Thermal radiation effects gained attention through the work of Jyothi et al. [7] who analyzed free convective flows over suddenly moved vertical plates. Using the Rosseland approximation for radiative heat transfer in gray, non-scattering media, they simplified the energy conservation equations while maintaining physical accuracy. Khan et al. [8] conducted a thorough review of passive thermal augmentation methods applicable to heat exchanger design, encompassing geometric modifications, surface treatments, and fluid property enhancements. The study systematically evaluated the thermal-hydraulic performance of various techniques considering practical implementation challenges and energy-efficiency criteria. Their work synthesized current research trends and identified promising directions for future investigations in passive heat transfer enhancement. This comprehensive analysis provides a valuable framework for optimizing heat exchanger performance in diverse engineering applications. Kodela Jyothi, et al. [9] offers a detailed analysis of transient free convection in electrically and thermally conducting water-based Casson nanofluid containing Copper (Cu)and Titanium dioxide (TiO_2) nanoparticles, flowing over an oscillating porous vertical plate. A constant transverse magnetic field is applied perpendicular to the flow, with thermal radiation and viscous dissipation incorporated into the energy equation.

The investigation of natural convection in porous media was advanced by Loganathan et al. [10] who established relationships between permeability, thermal Grashof numbers, and boundary layer thickness. Their results showed inverse correlations between Prandtl numbers and thermal-boundary-layer thickness and between Schmidt numbers and species-concentration boundary layers. Recent advances in nanofluid analysis include the work of Joby

Mackolil et al. [11] who employed statistical and analytical methods to examine unsteady radiative flows incorporating Dufour effects. Their comparative analysis of uniform heat flux (UHF) versus uniform wall temperature (UWT) boundary conditions revealed significant influences of Dufour effects on velocity and temperature profiles. The complexity of non-Newtonian nanofluid behavior was addressed by Macha Madhu et al. [12] who applied Maxwell fluid models to describe magnetohydrodynamic flows over stretching surfaces under radiation conditions. Their work employed variational finite element techniques to solve the resulting nonlinear differential equations. Md Atiqur Rahman, et al. [13] presents recent advances in the development, stability, thermo physical properties, and performance of nanofluids in thermal systems. A comprehensive literature review reveals significant progress in nanofluid technology. Researchers have demonstrated that the dispersion of nanoparticles in base fluids substantially enhances thermal properties, such as the heat transfer coefficient, thermal conductivity, and specific heat capacity. These modifications strongly influence key performance parameters, including the friction factor (f), Nusselt number, and pumping efficiency. Nanofluids are employed across diverse thermal applications depending on their thermophysical characteristics, with optimal operating conditions—such as temperature, nanoparticle volume fraction (), Furthermore, the use of nanofluids with a higher heat capacity than that of the base fluid significantly enhances the overall efficiency of thermal systems.

Muthucumaraswamy et al. [14] developed analytical solutions for steady-state heat and mass transfer over infinite vertical plates using Laplace transform methods. Their work established a baseline understanding of velocity and concentration profiles and examined the influence of buoyancy-to-viscous force ratios on transport phenomena. The intersection of Casson fluid behavior with porous media was explored by Oyekunle et al. [15] who examined viscous dissipation and chemical reaction effects in magnetohydrodynamic flows through vertical porous plates. Their collocation-based solutions revealed asymptotic behavior approaching Newtonian behavior for large Casson parameters. Radhakrishnan and Palani [16] conducted comprehensive studies on four different nanofluids (Cu, Al_2O_3, TiO_2, and Ag in water) under MHD conditions with heat sources, thermal radiation, and chemical reactions. Their findings established performance hierarchies among different nanoparticle types, with silver-water nanofluids showing maximum velocity profiles and Al_2O_3 -water nanofluids exhibiting maximum temperatures. Rajesh et al. [17] focused specifically on impulsive motion effects in nanofluid flows, employing implicit finite difference methods to analyze aluminum oxide, copper, titanium dioxide, and silver nanofluids with volume fractions up to 0.04. Their comprehensive parameter studies included nanoparticle volume fractions, magnetic parameters, and thermal Grashof numbers. Recent developments include Newtonian heating studies by Raju et al. [18] who obtained closed-form solutions using Laplace transforms for free convection flows over spontaneously started vertical surfaces.

Saha et al. [19] investigated the combined influence of thermal radiation and internal heat generation on magnetohydrodynamic flow behavior adjacent to a uniformly heated vertical surface. Their work examined how magnetic-field effects interact with radiative heat-transfer mechanisms during natural convection, which is of practical relevance to industrial thermal-processing systems. The study contributed to understanding the coupled effects of multiple physical phenomena on boundary layer characteristics in heat transfer applications involving conducting fluids. The emergence of nanofluids has attracted significant research attention due to their superior thermal properties and industrial applications. The incorporation of viscous dissipation effects was addressed by Suneetha Sangapatnam [20] who employed Crank-Nicolson finite difference methods to solve radiative heat transfer problems. Their results demonstrated acceleration effects due to increasing Eckert numbers and velocity reductions due to thermal radiation. Sarala and Geetha [21] performed a computational analysis of nanofluid convection over an oscillating plate subjected to magneto-hydrodynamic effects and Hall current phenomena. The investigation accounted for thermal radiation contributions while exploring the interplay between electromagnetic parameters and thermal transport mechanisms. Their numerical approach revealed important correlations among oscillation frequency, magnetic field intensity, and heat transfer enhancement characteristics. The study advances the understanding of coupled thermal-electromagnetic phenomena in nanofluid systems relevant to advanced cooling technologies.

Mathematical modeling of convective heat transfer in nanofluids has been significantly advanced by Buongiorno's comprehensive framework. Shehzad et al. [22] applied this mathematical model to investigate convective heat transfer characteristics of nanofluids flowing through wavy channels. Their analysis incorporated the effects of Brownian motion and thermophoresis, which are fundamental mechanisms governing nanoparticle behavior in fluid suspensions. The wavy channel geometry introduced additional complexity by enhancing mixing and augmentring heat transfer, providing insights for practical heat exchanger applications. The integration of magnetic field effects with thermal diffusion phenomena in nanofluid systems has received considerable attention for its potential to control heat transfer. The field has evolved toward hybrid nanofluid systems, as demonstrated by Suriya Uma Devi and Anjali Devi [25] who introduced novel thermophysical property models for Cu-Al_2O_3/water hybrid nanofluids. Their work established validated predictive models through comparison with experimental data, advancing both theoretical understanding and practical applications. Additionally, Mumukshu Trivedia et al. [26] investigated Jeffrey nanofluid flows with viscous dissipation and activation energy effects using multi-domain bivariate spectral quasi-linearization methods. Ubale Patil et al. [27] investigated the combined influence of mass transfer and heat generation on rotational fluid motion over an accelerating vertical surface embedded in a porous matrix. The study examined how rotation parameters interact with porous medium characteristics to modify momentum and energy transport mechanisms. Their numerical analysis revealed that increased rotational

effects significantly alter the velocity profiles and the development of the thermal boundary layer, while the porous-medium resistance dampens flow acceleration near the plate surface. Vijayakumar et al. [28] extended radiation analysis to exponentially accelerated vertical plates under variable temperature and mass diffusion conditions. Their comprehensive study revealed that magnetic parameters consistently reduce fluid velocity in both heating and cooling scenarios, while Soret numbers and viscous-to-mass diffusion ratios exhibit contrasting effects depending on thermal conditions. Hybrid nanofluids constitute the next generation of heat-transfer fluids, exhibiting higher thermal conductivity than conventional nanofluids. Hassan Waqas et al. [29] explored Fe_3O_4-CuO/H_2O hybrid nanofluids under magnetic field control, comparing performance against conventional CuO/H_2O nanofluids. Their research highlighted the synergistic effects of ferrofluid and copper oxide nanoparticles in water-based systems, demonstrating enhanced heat transfer across temperature gradients. The practical applications of these materials extend beyond heat transfer; ferro-based nanomaterials are used in manufacturing, protein synthesis, catalysis, and medicine. Copper oxide nanoparticles play specific roles in rocket propulsion systems by enhancing combustion rates and catalytic performance of ammonium perchlorate-based composite propellants.

The combined effects of thermophoresis, Brownian diffusion, and particle electrification on nanofluid flows with slip boundary conditions have not been examined previously. Sujit Mishra, et al. [24] investigated the steady, laminar natural convection of nanofluid flow past an isothermal vertical plate under slip boundary conditions. Buongiorno's revised four-equation non-homogeneous model is employed, incorporating thermophoresis, Brownian diffusion, and particle electrification. The study analyzes the effects of key parameters: the mass transfer coefficient increases with increasing Brownian motion and electrification parameters but decreases with the thermophoresis parameter. The proposed physical model has practical relevance in nanofluid-based heat exchangers and in the cooling of plate-shaped products during manufacturing processes. The novelty of this work lies in the simultaneous analysis of Brownian diffusion, thermophoresis, and particle electrification in nanofluid flow under slip boundary conditions.

Ashish Khudaiwala et al. [31] established research work on thermally manages high-wattage LED's. For this they have used a heat pipe with a screen mesh wick along with distilled water-based Cu and SiO_2 nanofluids. It has been observed that CuO-DI water-filled heat pipes are significantly effective compared to DI and SiO_2-DI water filled heat pipes for all types of LED's.

Mehdi Amiri et al. [32] studied synthesized iron oxide nanoparticles using Co-Precipitation method with exact size and distribution control. Two different samples 29.42 nm, NH_4OH and 38.04 nm, NaOH obtained. Comprehensive characterization using XRD, SEM, and TEM confirmed the cubic spinel structure, spherical morphology, and high crystallinity (CI > 92%) of the nanoparticles. Thermal performance evaluation discovered considerable enhancements in heat transfer.

Despite extensive research in nanofluid heat transfer enhancement, significant gaps remain in understanding the combined effects of impulsive motion, magnetic fields, and thermal radiation on copper nanoparticle-enhanced fluids over vertical surfaces. Nevertheless, existing literature lacks a comprehensive investigation of transient nanofluid behavior with non-uniform particle concentration under time-dependent thermal flux conditions. Current studies predominantly examine steady flows or uniform dispersion scenarios, overlooking the complex interactions during impulsive plate initiation. The simultaneous influence of spatially variable nanoparticle distribution, unsteady boundary layer development, and imposed heat flux on transport phenomena remains insufficiently understood. This knowledge deficit hinders the practical implementation of nanofluid systems in which concentration gradients and transient thermal loading occur simultaneously. Consequently, this investigation addresses this research gap by analyzing coupled heat and mass transfer mechanisms in unsteady nanofluid flows over impulsively started vertical plates. The findings provide essential guidance for optimizing nanofluid-based thermal applications under realistic operating conditions.

2. Flow configurations and physical model description

An infinite vertical plate with impulsive motion refers to a flat surface that extends infinitely in one direction and is set into motion instantaneously at a specific time. This study considers the motion of a viscous, incompressible nanofluid over an unsteady infinite vertical plate. The vertical direction alongside the plate is taken as one axis, x' while the direction normal to the plate is denoted as y' the other axis. The ambient Temperature in the undisturbed region of the fluid is represented by T_∞. Figure 1 illustrates the problem's physical configuration: an impulsively started vertical plate immersed in a copper nanoparticle-enhanced fluid subjected to a transverse magnetic field and it is adapted from R. Muthucumaraswamy et al. [30].

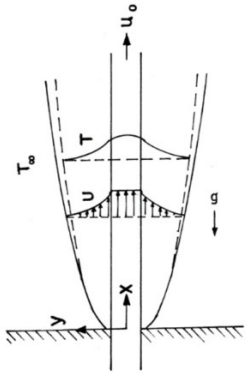

Figure 1. Schematic of the physical model and coordinate system

Initially, $t' \leq 0$ the fluid and the infinite vertical plate were maintained at similar, uniform thermal and solutal conditions resulting in a steady state. $t' > 0$ The plate is suddenly set into upward movement with x' a steady u_0 velocity. Simultaneously, invariant thermal and mass transfer rates are applied at the surface of the plate. In this study, copper nanoparticles are dispersed in water, to form a nanofluid. It is understood that the continuous phase (water), the suspended nanoparticles and the system are thermally stable and at rest.

Table 1. Relevant thermophysical parameters of copper–water nanofluid components

Physical Properties	Water/Base fluid	Copper
$\rho(kg/m^3)$	997.1	8933
$C_\rho(J/kgK)$	4179	385
$k(W/mK)$	0.613	401
$\beta \times 10^5(K^{-1})$	21	1.67
$\beta^* \times 10^6(m^2/h)$	298.2	3.05
ϕ	0.0	0.05
$\sigma(S/m)$	5.5×10^{-6}	

Table 1 lists the thermophysical properties of copper nanoparticles and water, which are commonly used in heat transfer and nanofluid research, and it is adopted from Chandra Reddy et al. [2]. These values may vary slightly depending on temperature, pressure, and particle size, but standard values at room temperature (around 25 °C or 298 K) are typically used.

Applying the classical Boussinesq approximation, the governing equations for flow past an unsteady infinite vertical plate are formulated following Chandrakala [3] and it is given as,

$$\rho_{nf}\frac{\partial u'}{\partial t'} = g(\rho\beta)_{nf}(T' - T'_\infty) + g(\rho\beta^*)_{nf}(C' - C'_\infty) + \mu_{nf}\frac{\partial^2 u'}{\partial y'^2} \quad (1)$$

$$(\rho C_\rho)_{nf}\frac{\partial T'}{\partial t'} = k_{nf}\frac{\partial^2 T'}{\partial y'^2} \quad (2)$$

$$\frac{\partial C'}{\partial t'} = D_{nf}\frac{\partial^2 C'}{\partial y'^2} \quad (3)$$

Here ' u' is the velocity part taken in the x-direction. The coefficient of the nanofluid is given as T the temperature. μ_{nf} the dynamic viscosity, ρ_{nf} the coefficient of thermal expansion, k_{nf} the density, the thermal conductivity. Also, g is the acceleration due to gravity and q_r is the radiative heat flux. The nanofluid's volumetric heat capacity is given by $(\rho C_p)_{nf}$.

Sujata Kalsi et al. [23] examined the Salient merits and limitations of nanofluids along with their potential applications in heat exchangers. Also, a comprehensive review of nanofluids with respect to their thermophysical properties and utilization in various engineering fields is discussed. The study developed a clear understanding of the key thermophysical characteristics of nanofluids, particularly thermal conductivity, viscosity, and specific heat capacity. The values of the nanofluid coefficients are expressed as follows:

$$\mu_{nf} = \frac{\mu_f}{(1-\phi)^{2.5}},\ \rho_{nf} = (1-\phi)\rho_f + \phi\rho_s$$

$$(\rho C_p)_{nf} = (1-\phi)(\rho C_p)_f + \phi(\rho C_p)_s$$

$$(\rho\beta)_{nf} = (1-\phi)(\rho\beta)_f + \phi(\rho\beta)_s \quad (4)$$

Here ϕ is the solid volume fraction of the nanosized particle. ρ_f base fluid density, ρ_s density of the nano-additive, μ_f the base fluid's viscosity, $(\rho C_\rho)_f$, thermal capacitance of the primary fluid and $(\rho C_\rho)_s$ the thermal capacitance of the nanoparticle. The terms in Equation (1) apply only to spherical nanoparticles. The other shapes of nanoparticles are not considered. The apparent thermal diffusivity of the fluid with nanoparticles is predicated by the Hamilton-Crosser model.

$$k_{nf} = k_f\left[\frac{k_s + 2k_f - 2/(k_f - k_s)}{k_s + 2k_f + /(k_f - k_s)}\right] \quad (5)$$

where k_f is the thermal conductivity of the fluid (W/m·K), which represents the fluid's ability to conduct heat through molecular motion and collisions and k_s is the nanoparticle's thermal conductivity in the system.

In the context of an optically thin gray gas, the radiative thermal rate is represented as

$$\frac{\partial q_r}{\partial y'} = -4a^*\sigma_f(T'^4_\infty - T'^4) \quad (6)$$

It is presumed that the temperature variations across the stream field are minimal. T'^4 can be described using a linear temperature dependence. Using Taylor's series T'^4 can be expressed with T'_∞ and truncating the expansion beyond leading terms, we have,

$$T'^4 \cong 4T'^3_\infty T' - 3T'^4_\infty \quad (7)$$

The subscripts nf in equations (1) to (5) denote the thermophysical properties of the nanofluid. Also, the subscripts f and s in equations (1) to (5) denote the respective combined thermophysical characteristics of the base fluid and dispersed nanosized particles.

With the following initial and boundary conditions:

$$\begin{aligned}
&t' \leq 0 \quad u' = 0, \quad T' = T'_\infty \quad C' = C'_\infty \quad \text{for all} \quad y' \leq 0,\\
&t' > 0: \quad u' = u_0 \quad \frac{\partial T'}{\partial y'} = -\frac{q}{K} \quad C = C'_\infty + (C'_w - C'_\infty)At' \quad \text{at} \quad y' = 0,\\
&\qquad\quad u' \to 0 \quad T' \to T'_\infty \quad C' \to C'_\infty \quad \text{as} \quad y' \to \infty
\end{aligned} \quad (8)$$

Using the non-dimensional quantities,

$$U = \frac{u'}{u_0} \qquad Y = \frac{y' u_0}{v_f} \qquad A = \frac{u_0^2}{v_f} \qquad Pr = \frac{\mu C_p}{k_f}$$

$$\theta = \frac{T' - T'_\infty}{\left(\frac{q v_f}{K_f u_0}\right)} \qquad C = \frac{C' - C'_\infty}{(C'_w - C'_\infty)} \qquad Sc = \frac{v_f}{D_f}$$

$$Gr = \frac{g\beta v_f \left(\frac{q v_f}{K_f u_0}\right)}{u_0^3} \qquad Gc = \frac{g\beta^* v_f \left(\frac{j'' v_f}{D_f u_0}\right)}{u_0^3} \qquad K_f = \frac{v_f k_{nf}}{u_0^2} \tag{9}$$

By using equations (4) and (5), equations (1) to (3) reduce to

$$L_1 \frac{\partial U}{\partial t} = L_3 \frac{\partial^2 U}{\partial Y^2} + L_2 Gr\theta + L_4 GcC$$

$$L_5 \frac{\partial \theta}{\partial t} = L_6 \frac{1}{Pr} \frac{\partial^2 \theta}{\partial Y^2}$$

$$\frac{\partial C}{\partial t} = \frac{1}{Sc} \frac{\partial^2 C}{\partial Y^2} \tag{10}$$

Where

$$L_1 = (1 - \phi) + \phi\left(\frac{\rho_s}{\rho_f}\right) \qquad L_2 = (1 - \phi) + \phi\left(\frac{(\rho\beta)_s}{(\rho\beta)_f}\right)$$

$$L_3 = \frac{1}{(1 - \phi)^{2.5}} \qquad L_4 = (1 - \phi) + \phi\left(\frac{(\rho\beta^*)_s}{(\rho\beta^*)_f}\right)$$

$$L_5 = (1 - \phi) + \phi\left(\frac{(\rho C_p)_s}{(\rho C_p)_f}\right) \qquad L_6 = \left[\frac{k_s + 2k_f - 2\phi(k_f - k_s)}{k_s + 2k_f + \phi(k_f - k_s)}\right] \tag{11}$$

The relevant initial and boundary conditions are as follows.

$$\begin{array}{llll} & U=0, \quad \theta=0, & C=0, & \forall\, y \le 0 \\ t > 0: & U=1, \quad \frac{\partial \theta}{\partial y} = -1, & C=t & \text{at } y=0 \\ & U \to 0 \quad \theta=0, & C \to 0 & \text{as } y \to \infty \end{array} \tag{12}$$

3. Solution procedure

The simultaneous linear equations with partial differential coefficients (10) to (12) are evaluated under the specific limit conditions given in equation (14) using the standard analytical Laplace transform procedure. Exponential and complementary error functions appear in the closed-form solutions (erfc). These analytical solutions capture the transient behavior of velocity, temperature, and concentration fields. The relationship connecting the error function erf(x) and its complementary error function erfc(x) is given by

$$erfc(x) = 1 - erf(x) \tag{13}$$

Using the Laplace transform technique, the dimensionless governing equations given in equation (10), subject to the limiting conditions specified in equation (12), were solved analytically. The analytical expressions for concentration, temperature, and velocity distributions are presented in Equations (14), (15), and (16) respectively.

$$C(t) = t\left[(1 + 2\eta^2 Sc)\,erfc(\eta\sqrt{Sc}) - \frac{2\eta\sqrt{Sc}}{\sqrt{\pi}} \exp(-\eta^2 Sc)\right] \tag{14}$$

$$\theta(t) = 2\sqrt{t}\left[\frac{\exp(-\eta^2 a)}{\sqrt{\pi}\sqrt{a}} - \eta\, erfc(\eta\sqrt{a})\right] \tag{15}$$

$$\begin{aligned} U(t) = erfc(\eta\sqrt{g}) & - \frac{L_2 G_r t\sqrt{t}}{3L_3\sqrt{a}(g - a)}\left[\frac{4}{\sqrt{\pi}}(1 + g\eta^2)\exp(-g\eta^2) - \eta\sqrt{g}(6 + 4g\eta^2)\,erfc(\eta\sqrt{g})\right] \\ & - \frac{L_4 G_c t^2}{3L_3(g - Sc)}\left[(3 + 12g\eta^2 + 4\eta^4 g^2)\,erfc(\eta\sqrt{g}) - \frac{\eta\sqrt{g}}{\sqrt{\pi}}(10 + 4g\eta^2)\exp(-g\eta^2)\right] \\ & + \frac{L_2 G_r t\sqrt{t}}{3L_3\sqrt{a}(g - a)}\left[\frac{4}{\sqrt{\pi}}(1 + a\eta^2)\exp(-a\eta^2) - \eta\sqrt{a}(6 + 4a\eta^2)\,erfc(\eta\sqrt{a})\right] \\ & + \frac{L_4 G_c t^2}{3L_3(g - Sc)}\left[(3 + 12Sc\eta^2 + 4\eta^4 (Sc)^2)\,erfc(\eta\sqrt{Sc}) - \frac{\eta\sqrt{g}}{\sqrt{\pi}}(10 + 4Sc\eta^2)\exp(-Sc\eta^2)\right] \end{aligned} \tag{16}$$

where

$$a = \frac{L_5 P_r}{L_6}, g = \frac{L_1}{L_3}, \eta = \frac{y}{2\sqrt{t}}$$

4. Results and discussions

The analysis is done for several dimensionless factors, such as the Schmidt number on velocity profiles, concentration profiles, temperature profiles, Prandtl number, mass Grashof number, and thermal Grashof number. In nanofluid studies, parameters **such as the solid volume** fraction**, thermal** conduc**tivity, and** Grashof number significantly influence heat and mass transport. Such analysis informs the **selection of nanoparticle** types **and base** fluids for targeted applications such as solar collectors, electronics cooling, and biomedical devices.

4.1. Significance of velocity profiles

The velocity profiles for nanofluid flow past an impulsively started vertical plate illustrate temporal variations in fluid velocity. It varies over time. The velocity field changes when the sudden plate motion and buoyancy effects brought on by temperature and concentration variations in this setting, occur, a situation usually evaluated under unstable natural or mixed convection. The Grashof number range ($Gr = 10^4$-10^6) is selected to ensure buoyancy-driven natural convection dominates while maintaining laminar flow conditions, representing typical industrial heat transfer applications on vertical surfaces. The Prandtl number range (Pr = 0.7 -7.0) encompasses common working fluids, from air to water-based systems, covering the spectrum of momentum-to-thermal diffusivity ratios encountered in practical engineering applications. At lower thermal Grashof numbers, the fluid flow decreases because the buoyancy forces driving natural convection become weaker relative to the viscous forces resisting motion. Lower Gr indicates reduced temperature differences between the plate and the ambient fluid, resulting in diminished density variations and weaker thermal expansion effects that propel the fluid upward along the vertical surface. Consequently, viscous forces dominate over buoyancy forces, creating greater resistance to fluid acceleration and leading to slower flow velocities and reduced momentum boundary layer development.

The key role of the mass Grashof number in the flow velocity pattern is shown in Figure 2 for the plate's thermal regimes during heating and cooling. The mass Grashof number is a dimensionless number that characterizes natural convection driven by concentration differences rather than by temperature differences. It compares the buoyant force caused by concentration variations with the fluid frictional force. At this juncture, the velocity distribution for some values of the mass Grashof number is examined while keeping all other parameters constant. The solid volume fraction is 0.05, the thermal Grashof number is 2, and the Prandtl number is 0.71. The Schmidt number was set to 0.66 per unit time. When the plate cools, the results indicate a rise in velocity and an increase in the Grashof number for mass transfer. However, when the plate is heated, the reverse phenomenon occurs. As the plate is heated, the velocity decreases because the Grashof number decreases. For both thermal conditions (i.e., thermal regulation of the plate) the velocity initially decreases to a minimum and then gradually approaches an asymptotic state.

Figure 3 depicts the same scenario. Also, when the fluid velocity increases the Grashof number for heat transfer increases. The Grashof number for heat transfer is a dimensionless number that characterizes free convection due to temperature differences in a fluid. It compares the buoyancy forces to viscous forces in the fluid. At time t=1, the parameters are set as follows: solid volume fraction = 0.05, mass Gc = 2, Pr = 0.71, and Sc = 0.66. An increased Gr enhances buoyancy forces, leading to higher fluid velocity under cooling plate conditions. Conversely, a lower thermal Grashof number reduces the fluid flow speed when the plate is heated.

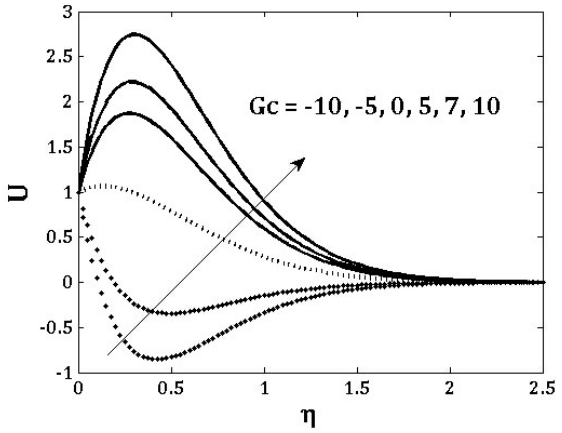

Figure 2. Effect of Gc on the velocity field

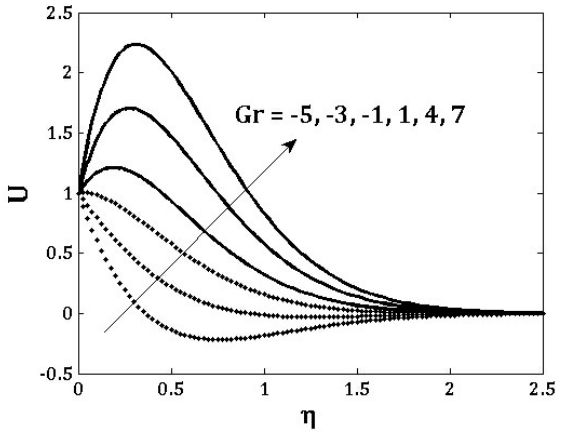

Figure 3. Effect of Gr on the velocity field

The Pr number represents the relative rates at which momentum and heat diffuse through a fluid and is the ratio of viscous to thermal diffusivity. In Figure 4, as the Prandtl number increases, indicating slower thermal diffusion, the corresponding velocity distribution weakens. As the viscous-to-thermal diffusivity ratio, known as the

Prandtl number, increases, the diffusion of heat decreases, meaning heat diffuses more slowly compared to momentum. This leads to a thinner thermal boundary layer but does not significantly affect the depth of the layer. By observation, a higher Prandtl number may indirectly cause a slight decrease in the velocity profile, whereas a lower Prandtl number implies higher thermal diffusivity, which may slightly enhance the velocity near the surface due to stronger thermal effects propagating into the fluid.

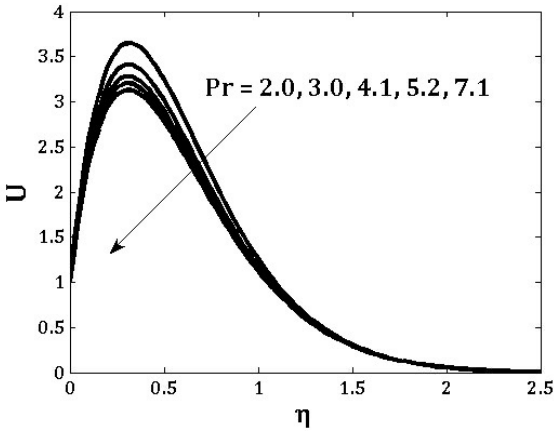

Figure 4. Effect of Pr number on the velocity field

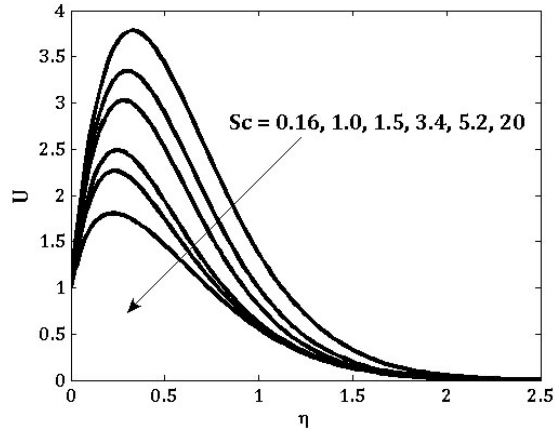

Figure 5. Effect of Sc number on the velocity field

Similarly, Figure 5 shows that increasing the Schmidt number (Sc) reduces the velocity profile. This behavior is supported by the fact that a higher Schmidt number corresponds to lower mass diffusivity, thereby reducing species diffusion within the boundary layer. Consequently, the buoyancy forces arising from concentration gradients are weakened, leading to a decline in fluid velocity. At higher Schmidt numbers, velocity decreases. When the Schmidt number decreases, flow velocity increases because mass diffusivity is enhanced, which further promotes species diffusion and strengthens buoyancy effects in the region adjacent to the surface.

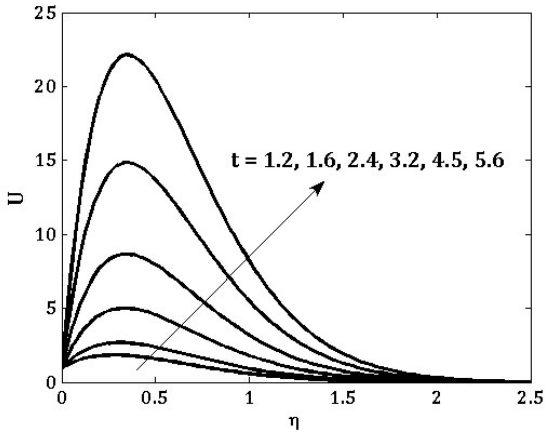

Figure 6. Effect of time on velocity field

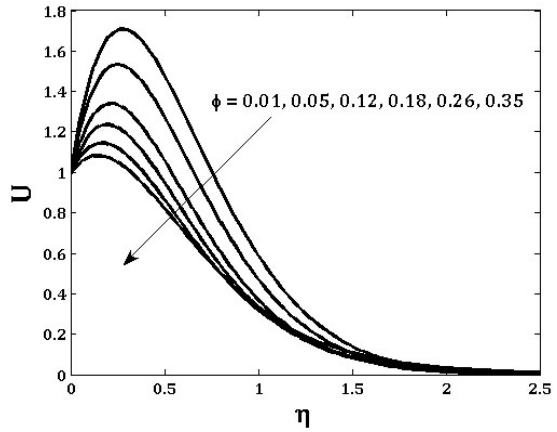

Figure 7. Effect of ϕ on velocity field

When the speed of fluid flow increases with time, a boundary layer develops, and momentum penetrates deeper into the fluid domain. This phenomenon is clearly shown in Figure 6. Initially, the fluid is at rest, and as time progresses, the flow evolves, resulting in a broader and more pronounced velocity distribution. Also, from Figure 7, we can observe that when the solid volume fraction of nanosized particles increases, it typically results in a decrease in fluid flow velocity because the presence of additional solid particles in the base fluid increases the effective viscosity of the nanofluid. Increased viscosity enhances resistance to flow, thereby suppressing fluid motion and reducing velocity. For both the time and solid volume fractions, the Prandtl number is set to 0.71. Likewise, the Schmidt number is taken as 0.66, and the Gr and Gc numbers are 3 and 2 respectively.

4.2. Significance of temperature profiles

A temperature profile shows how heat spreads from a surface (e.g., a heated or cooled plate) into the surrounding fluid. It is typically a function of the distance from the surface (y) and of time (t), especially in unsteady flow. When a vertical plate is suddenly heated or cooled, heat diffuses into the fluid forming a thermal boundary lay-

er. The temperature profile shows how the fluid temperature changes with distance from the plate. Some common factors that affect the temperature profile are Prandtl number, thermal diffusivity, time, and the condition of the vertical plate. Figure 8 shows that, when unit time, a particle size of 0.05, and a Schmidt number of 0.66 are considered, the temperature profile decreases as the Prandtl number rises. This occurs because of reduced thermal diffusivity, limiting heat conduction into the fluid. This occurs because a higher Prandtl number corresponds to a lower thermal diffusivity, meaning that heat diffuses more slowly than momentum. As a result, the fluid layer adjacent to a solid surface becomes thinner, and heat produced within the fluid decreases more rapidly with distance from the surface. In unsteady (time-dependent) heat transfer problems, time plays a key role in determining how the temperature profile evolves within the boundary. Figure 9 illustrates that as time progresses; the thermal profile becomes more pronounced due to increased thermal diffusion. This causes a temperature rise far from the plate, increasing the thickness of the boundary layer. During the initial stage, heat affects only the fluid near the plate, producing a steep temperature gradient; in the later stage, heat penetrates deeper, producing a broader temperature profile and higher temperatures.

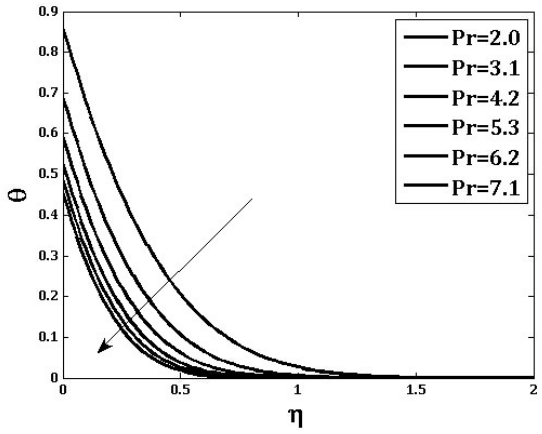

Figure 8. Effect of Pr on temperature field

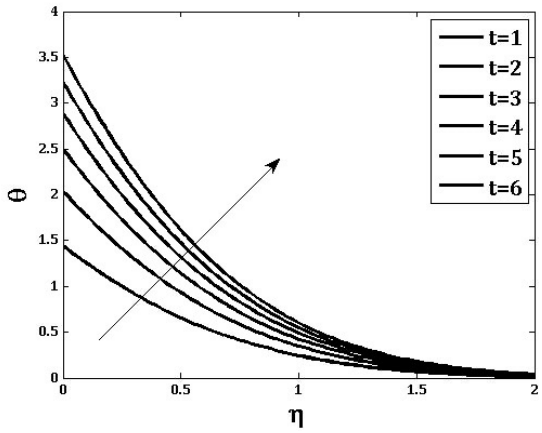

Figure 9. Effect of time on temperature field

Figure 10 shows that the solid-volume segment in the temperature profile is caused by an increase in solid-particle size, which leads to a rise in temperature. This occurs because nanoparticles typically have higher thermal conductivity than the base fluid, enhancing the fluid's ability to transfer heat. As a result, the thermal boundary layer thickens, and the temperature increases throughout the fluid domain.

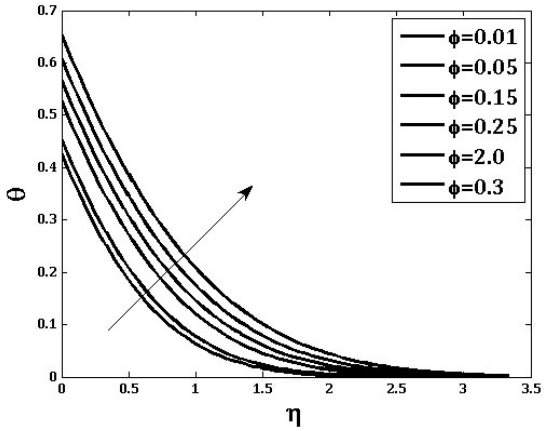

Figure 10. Effect of ϕ the temperature field

4.3. Significance of concentration profile

A concentration profile describes how the concentration of a species or solute varies with position (usually in the direction normal to a surface) in a fluid flow or diffusion process. A concentration profile describes how a solute spreads in a fluid. It is dependent on the boundary conditions (e.g., plate concentration), Schmidt number (Sc), and time (in unsteady cases). Usually, it is used to calculate the Sherwood number (Sh), which measures the mass transfer rate. This profile reflects how the concentration of nanoparticles in the fluid evolves over time due to mass-transfer effects.

The dimensionless number represents the relative magnitudes of momentum and mass diffusion characterizes momentum diffusivity (viscosity) relative to mass diffusivity. It plays a crucial role in mass transfer behavior, especially in boundary layer flows. Figure 11 shows that as the Schmidt number increases, mass diffusivity decreases, leading to slower diffusion of species in the liquid. Therefore, the concentration boundary layer becomes thinner. The concentration profile decreases more rapidly with increasing distance from the surface. The concentration profile increases significantly over time, as shown on Figure 12. As time progresses, the concentration boundary layer thickens due to enhanced mass diffusion, resulting in increased concentrations farther from the wall. Here, the particle size is set to 0.05. The Prandtl and Schmidt numbers are constant at 0.71 and 0.6, respectively. When time is minimal, a sharp concentration gradient near the wall, that is, a thin boundary layer is observed; when time is maximal, a broader spread in the fluid produces a gradual concentration gradient.

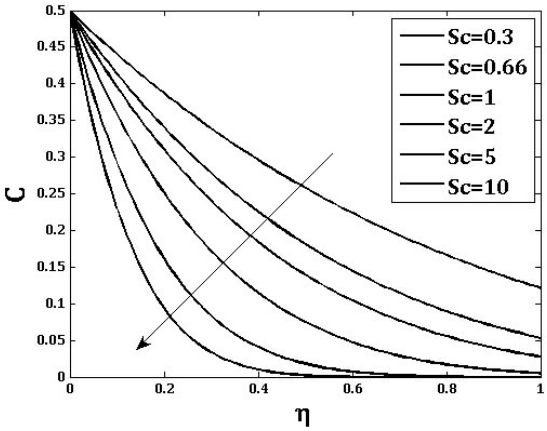

Figure 11. Effect of Sc on concentration field

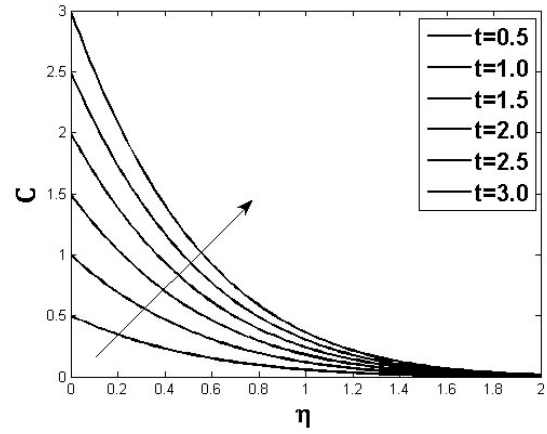

Figure 12. Effect of time on the concentration field

4.4. Assessment of parameters influencing convective heat and mass transfer

Evaluating the impact of key parameters on thermal and mass transport is crucial for understanding, optimizing, and predicting the behavior of thermal and solutal transport phenomena in fluid systems. By identifying parameters that increase the Nusselt or Sherwood numbers, engineers can design more efficient cooling, heating, drying, or mixing systems. For example, increasing the Prandtl number (via fluid selection) or the solid volume fraction in nanofluids can significantly enhance heat transfer performance. Understanding how variables such as the Grashof number, the Schmidt number, and nanoparticle concentration affect transfer rates help create accurate mathematical models. This is essential for simulations, control systems, and scaling of laboratory results to industrial applications. Systems such as heat exchangers, chemical reactors, and cooling devices depend heavily on heat and mass transfer characteristics. Parameter assessment helps select appropriate operating conditions and geometries to maximize performance. In nanofluid studies, parameters like solid volume fraction, thermal conductivity, and Grashof number significantly influence heat/mass transport. Such analysis informs the selection of nanoparticle types and base fluids for targeted applications like solar collectors, electronic cooling, or biomedical devices.

The Sherwood number (Sh) is the ratio of convective mass transfer to diffusive mass transfer at a surface or interface in a fluid system. It predicts mass-transfer rate in processes such as drying, evaporation, absorption, corrosion, and chemical reactions. It is used in biomedical, chemical, food, and environmental engineering to design and optimize systems.

$$\mathrm{Sh} = -\left(\frac{\partial C}{\partial \eta}\right)_{\eta=0}$$

In Table 2, when the Sherwood number is greater than one, then the convective mass transport dominates over diffusion. If the Sherwood number equals one, then no convection takes place. Instead, we will observe pure diffusion. Also, if the number is less than one, it usually indicates weak convection.

Table 2. Variation of Sherwood number with controlling factors

t	Sc	Sh	t	Sc	Sh
0.1	0.6	0.1748	0.1	0.1	0.0714
0.5		0.8740		0.5	0.1596
1		1.7481		1	0.2257
1.2		2.0977		2	0.3192
1.5		2.6221		6	0.5528
2		3.4962		15	0.8740

The table below indicates that the dimensionless Sherwood number increases over time. Additionally, it increases with Sc number. From the given values, convective mass transfer dominates mass diffusion when time exceeds one. However, for times less than one, even at higher Schmidt numbers, the Sherwood number remains below unity, indicating that convection is weak and diffusion is the dominant mechanism.

Table 3. Enhanced table with comparison of sherwood number

t	Sc	Present Study (Sh)	Muthucumaraswamy et al. [14] (Sh)	Relative Error (%)
0.1	0.6	0.1748	0.1745	0.171624714
0.5	0.6	0.8740	0.8735	0.057208238
1	0.6	1.7481	1.7475	0.034322979
1.2	0.6	2.0977	2.0970	0.033369881
1.5	0.6	2.6221	2.6215	0.022882422
2	0.6	3.4962	3.4955	0.020021738
0.1	0.1	0.0714	0.0712	0.280112045
0.1	0.5	0.1596	0.1594	0.125313283
0.1	1	0.2257	0.2255	0.088613203
0.1	2	0.3192	0.3190	0.062656642
0.1	6	0.5528	0.5526	0.03617945
0.1	15	0.8740	0.8738	0.022883295

Table 3 presents a quantitative validation of the current Sherwood number results against the established benchmark data from Muthucumaraswamy et al. [14] for varying Schmidt numbers and time parameters. The excellent agreement between the present analytical solutions confirms the accuracy and reliability of the proposed mathematical model, with maximum deviations remaining within acceptable limits for engineering applications.

The skin-friction coefficient measures the viscous resistance that a fluid flow exerts tangentially on a solid boundary. It is critical for analyzing flow efficiency, energy losses, and surface drag across a broad range of engineering systems. The coefficient of skin friction is highly sensitive to fluid properties, flow conditions, and external forces. Each parameter either intensifies or dampens the velocity gradient at the surface, directly affecting wall shear stress.

$$c_f = -\left(\frac{\partial U}{\partial \eta}\right)_{\eta=0}$$

Table 4 shows that as particle size increases, the skin-friction coefficient increases, largely due to enhanced viscous effects and momentum-transfer resistance near the wall. Larger nanoparticles increase the effective viscosity of the nanofluid. Additionaly, larger particles increase resistance to fluid motion, especially near the surface. This resistance increases the velocity gradient at the wall, which in turn increases the drag coefficient. The table shows that larger drag coefficients are associated with higher Prandtl numbers. In many classical cases, increasing the Prandtl number (Pr) tends to decrease skin friction due to thinner velocity boundary layers. But in nanofluid flows over cooling plates, or in impulsively started flows, it may be observed that with an increasing Prandtl number, the wall shear stress rises and the dynamic pressure of the free stream decreases. This is one of the reasons why nanoparticles alter both thermal and momentum diffusion; therefore, increased Pr in nanofluids, due to changes in thermal conductivity or specific heat, can lead to a coupled enhancement of flow and shear stress.

Also, from the table below, we observe that, as time increases, the skin-friction coefficient decreases in unsteady boundary-layer flows due to the reduction in wall shear caused by the growth of the velocity boundary layer. Also, initial acceleration causes high shear that results in very steep velocity gradients close to the wall, which induces a high drag force, and in turn, we get a high skin friction coefficient. The table above shows that an increase in the Schmidt number raises the skin-friction coefficient, particularly in flows in which concentration gradients drive buoyancy forces or couple with momentum transfer. The Grashof number increases, and skin friction decreases under heating conditions.

Table 4. Values of wall shear coefficient

ϕ	t	Pr	Sc	Gr	Gc	C_f
0.01	0.1	7.1	0.66	2	3	1.1035
0.02						1.1310
0.03						1.1560
0.04						1.1788
0.05						1.1994
0.15						1.3147
0.05	0.2	7.1	0.66	2	3	1.0583
	0.3					0.8316
	0.4					0.5205
	0.5					0.1259
	0.6					-0.3518
	1.0					-3.0872
0.05	0.1	2.0	0.66	2	3	1.1772
		3.1				1.1873
		4.2				1.1926
		5.3				1.1959
		6.2				1.1979
		7.56				1.2000
0.05	0.1	7.1	0.16	2	3	1.1886
			0.66			1.1994
			1			1.2029
			2.4			1.2103
			3.5			1.2134
			6			1.2175
0.05	0.1	7.1	0.66	1	3	1.2056
				3		1.1932
				5		1.1807
				7		1.1683
				11		1.1434
				15		1.1185
0.05	0.1	7.1	0.66	2	2	1.2125
					3.5	1.1928
					5	1.1731
					7	1.1468
					11	1.0942
					15	1.0416

5. Conclusion

This investigation offers valuable perspectives on enhancing nanofluid utilization in transient thermal systems, particularly for microscale cooling applications and thermal energy storage solutions. When nanofluids flow along a vertical surface with elevated solute concentrations at the wall than in the bulk fluid, mass diffuses outward. The findings demonstrate that elevated nanoparticle concentrations lead to substantial improvements in both thermal boundary layer characteristics heat transfer performance, while impulsive initiation significantly affects the evolution of the flow structure adjacent to the surface.

- Enhanced thermal Grashof numbers are associated with the increased fluid velocities as intensified temperature gradients strengthen buoyancy-driven motion. Correspondingly, elevated mass Grashof numbers increased flow velocities via concentration-induced buoyancy. Elevated Prandtl numbers result in a reduced velocity profile, higher Prandtl values indicate diminished thermal

diffusion compared to momentum diffusion, leading to narrower thermal boundary layers and reduced penetration of thermal energy into the fluid region. Increasing Schmidt numbers correlate with a reduction in the velocity profile because higher Schmidt numbers indicate decreased mass diffusivity.

- Velocity profiles generally increase over time, particularly during the initial unsteady flow phases. Initially, the fluid adjacent to the boundary accelerates due to the sudden motion of the plate. Subsequently, velocity profiles may reach equilibrium as flow transitions toward quasi-steady or steady conditions, depending on boundary specifications. Rising solid volume fractions increase effective viscosity and nanofluid density. This increases internal flow resistance, thereby inhibiting fluid motion. Consequently, boundary-layer velocities decrease as additional nanoscale particles are incorporated into the base fluid.
- Temperature distributions decrease with increasing Prandtl numbers because thermal diffusion is increasingly restricted relative to momentum transport, yielding thinner thermal boundary layers and reduced near-wall temperatures. The temporal evolution reveals progressive increase in temperature as impulsive surface heating effects propagate deeper into the fluid domain. Higher nanoparticle volume fractions enhance temperature distributions by increasing the effective thermal conductivity, thereby strengthening heat transfer mechanisms thought the system.
- Enhanced Sherwood numbers confirm the predominance of convective mass transport over diffusive transport mechanisms at boundary interfaces. Skin friction coefficients exhibit positive correlations with the Prandtl number, the Schmidt number, and nanoparticle loading, while showing inverse relationships with time and Grashof parameters.

For microscale cooling systems, optimal performance requires balancing the nanoparticle concentration (recommended 2-4% volume fraction) to maximize thermal conductivity gains while mitigating viscosity-induced pressure penalties. In transient thermal storage applications, strategic selection of Prandtl and Schmidt numbers enables precise control over thermal and concentration boundary layer thicknesses. Impulsive startup protocols should account for the time-dependent evolution of velocity and temperature with stabilization periods ranging from dimensionless time t = 0.5-1.0 in most configurations. These findings provide quantitative guidelines for nanofluid-based heat exchanger design, electronics cooling systems, and renewable energy storage optimization.

Acknowledgement

I am grateful to Dr. E. Geetha, Assistant Professor, Sri Chandra Sekharendra Saraswati Viswa Maha Vidyalaya, Enathur, Kanchipuram, for her meticulous guidance and unconditional support throughout the completion of this paper. Her valuable insights, encouragement, and constant supervision were instrumental in shaping the quality and direction of this work.

Nomenclature

List of symbols

c'	Species Concentration near the plate. [kg/m³]
c'_∞	Species Concentration in the fluid far away from the plate [kg/m³]
C	Dimensionless concentration.
C_p	Specific heat at constant pressure [J/kg·K]
D	Mass diffusion coefficient [m²/s]
g	Acceleration due to gravity [m/s²]
Gr	Thermal Grashof number
Gc	Mass Grashof number
K	Thermal conductivity of the fluid [W/m·K]
Pr	Prandtl number
q	Heat flux per unit area at the plate [W/m²]
Nu	Nusselt number
Sc	Schmidt number
Sh	Sherwood number
C_f	Skin friction coefficient
t'	time [s]
t	time [s]
T'	Temperature of the fluid near the plate [K]
T'_∞	The temperature of the fluid far away from the plate [K]
T'_w	Temperature of the plate [K]
u'	Velocity of the fluid in the x' - direction [m/s]
u_0	Velocity of the plate [m/s]
u	Dimensionless velocity
x'	Coordinate axis along the plate [m]
y'	Coordinate axis normal to the plate [m]
y	Dimensionless coordinate axis normal to the plate
β	Thermal coefficient of thermal expansion [1/K]
β*	Volumetric coefficient of expansion with concen tration [m³/kg]
μ	Coefficient of viscosity [kg/ms]
v	Kinematic viscosity [m²/s]
ρ	Density [kg/m³]
c_f	Skin-friction [N/m²]
θ	Dimensionless temperature
erfc	Complementary error function
η	Similarity parameter

References

[1] Banerjee, S. K. Mahato, K. Bhattacharyya, S. Rajput, A. K. Verma, and A. J. Chamkha, "Insight of boundary layer structure with heat transfer through a diverging porous channel in Darcy–Forchheimer porous material with suction/injection: A study of separation control," Journal of Thermal Engineering, vol. 9, no. 6, pp. 1419–1427, 2023.

[2] Chandra Reddy, M. C. Raju, G. S. S. Raju, and S. V. K. Varma, "Free convective magneto-nanofluid flow past a moving vertical plate in the presence of radiation and thermal diffusion," Frontiers in Heat and Mass Transfer, vol. 7, Art. no. 28, 2016, DOI: 10.5098/hmt.7.28.

[3] Chandrakala, "Effects of chemical reaction on MHD flow past an impulsively started infinite vertical plate with uniform heat and mass flux," International Journal of Applied Mechanics and Engineering, vol. 18, no. 2, pp. 329–339, 2013, DOI: 10.2478/ijame-2013-0019.

[4] Djebali, F. Mebarek-Oudina, and C. Rajashekhar, "Similarity solution analysis of dynamic and thermal boundary layers: Further formulation along a vertical flat plate," Physica Scripta, vol. 96, no. 8, 2021.

[5] A. Duguma, O. D. Makinde, and L. G. Enyadene, "Dual solutions and stability analysis of Cu–H_2O-Casson nanofluid convection past a heated stretching/shrinking slippery sheet in a porous medium," Computational and Mathematical Methods, vol. 2023, Art. no. 6671523, 2023, https://doi.org/10.1155/2023/6671523.

[6] Hayat and S. Nadeem, "Heat transfer enhancement with Ag–CuO/water hybrid nanofluid," Results in Physics, vol. 7, pp. 2317–2324, 2017, http://dx.doi.org/10.1016/j.rinp.2017.06.034.

[7] Jyothi, P. Lalitha, and R. L. V. Renuka Devi, "Thermal radiation effects on flow past an impulsively started vertical moving plate with uniform heat and mass flux," International Journal of Advanced Research in Computer Science, vol. 8, no. 6, pp. 69–73, 2017.

[8] A. Khan, M. Ilyas, K. Waheed, I. Haq, and F. Aydogan, "Advances in passive heat transfer enhancement for heat exchangers: A comprehensive review," Journal of Thermal Engineering, vol. 11, no. 4, pp. 1193–1230, 2025.

[9] Jyothi and V. C. S. Kasulanat, "Unsteady MHD Casson Nanofluid Flow Past a Porous Moving Vertical Plate with Heat Sink," Journal of Advanced Research in Fluid Mechanics and Thermal Sciences, vol. 133, no. 1, pp. 137–155, 2025.

[10] Loganathan and C. Sivapoornapriya, "Unsteady heat and mass transfer effects on an impulsively started infinite vertical plate in the presence of porous medium," International Journal of Heat and Technology, vol. 33, no. 2, pp. 1–8, 2015. http://dx.doi.org/10.18280/ijht.330211

[11] Mackolil and B. Mahanthesh, "Exact and statistical computations of the radiated flow of nano and Casson fluids under heat and mass flux conditions," Journal of Computational Design and Engineering, vol. 6, pp. 593–605, 2019, https://doi.org/10.1016/j.jcde.2019.03.003.

[12] Madhu, N. Kishan, and A. J. Chamkha, "Unsteady flow of a Maxwell nanofluid over a stretching surface in the presence of magnetohydrodynamic and thermal radiation effects," Propulsion and Power Research, vol. 6, no. 1, pp. 31–40, 2017, http://dx.doi.org/10.1016/j.jppr.2017.01.002

[13] A. Rahman, S. M. M. Hasnain, S. Pandey, A. Tapalova, N. Akylbekov, and R. Zairov, "Review on Nanofluids: Preparation, Properties, Stability, and Thermal Performance Augmentation in Heat Transfer Applications," ACS Omega, vol. 9, no. 30, pp. 32328–32349, 2024, https://doi.org/10.1021/acsomega.4c03279.

[14] Muthucumaraswamy, P. Ganesan, and V. M. Soundalgekar, "Heat and mass transfer effects on flow past an impulsively started vertical plate," Acta Mechanica, vol. 146, pp. 1–8, 2001, DOI: 10.1007/BF01178790.

[15] L. Oyekunle, M. T. Akolade, and S. A. Agunbiade, "Thermal-diffusion and diffusion-thermo effects on heat and mass transfer in chemically reacting MHD Casson nanofluid with viscous dissipation," Applied and Applied Mathematics, vol. 16, no. 1, pp. 705–723, 2021.

[16] Radhakrishnan and G. Palani, "Impact of MHD and nanofluid flow through a vertical plate with varying heat and mass flux," Journal of Naval Architecture and Marine Engineering, vol. 21, pp. 15–26, 2024, http://dx.doi.org/10.3329/jname.v21i1.55428.

[17] Rajesh, A. J. Chamkha, and M. P. Mallesh, "Transient MHD free convection flow and heat transfer of nanofluid past an impulsively started semi-infinite vertical plate," Journal of Applied Fluid Mechanics, vol. 9, no. 5, pp. 2457–2467, 2016, DOI:10.18869/acadpub.jafm.68.236.23443.

[18] V. S. Raju, T. S. Reddy, M. C. Raju, S. Venkataraman, and S. V. K. Varma, "Heat and mass transfer effects on unsteady free convection boundary layer flow past an impulsively started vertical surface with Newtonian heating," International Journal of Scientific Research, vol. 2, no. 2, pp. 1–8, 2013.

[19] Saha, T. Sultana, and S. Saha, "Effect of thermal radiation and heat generation on MHD flow past a uniformly heated vertical plate," Desalination and Water Treatment, vol. 16, pp. 57–65, 2010, doi no. 10.5004/dwt.2010.1086.

[20] Sangapatnam, B. R. Nandanoor, and V. R. P. Vallampati, "Radiation and mass transfer effects on MHD free convection flow past an impulsively started isothermal vertical plate with dissipation," Thermal Science, vol. 13, no. 2, pp. 171–181, 2009, DOI: 210.2298/TSCI0902171S.

[21] Sarala and E. Geetha, "Numerical analysis of nanofluid flow over a radiating oscillating plate with Hall current and MHD at enhanced temperature," Journal of Thermal Engineering, vol. 11, pp. 127–140, 2025.

[22] Shehzad, A. Zeeshan, R. Ellahi, and K. Vafai, "Convective heat transfer of a nanofluid in a wavy channel: Buongiorno's mathematical model," Journal of Molecular Liquids, vol. 222, pp. 446–455, 2016, http://dx.doi.org/10.1016/j.molliq.2016.07.052.

[23] Kalsi, S. Kumar, A. Kumar, T. Alam, and D. Dobrota, "Thermophysical properties of nanofluids and their potential applications in heat transfer enhancement: A review," Arabian Journal of Chemistry, vol. 16, Art. no. 105272, 2023, https://doi.org/10.1016/j.arabjc.2023.105272.

[24] Mishra, A. K. Pati, A. Misra, and S. K. Mishra, "Thermal performance of nanofluid flow along an isothermal vertical plate with velocity, thermal, and concentration slip boundary conditions employing Buongiorno's revised non-homogeneous model," East European Journal of Physics, vol. 4, pp. 98–106, 2024.

[25] U. Devi and S. P. Anjali Devi, "Heat transfer enhancement of Cu–Al_2O_3/water hybrid nanofluid flow over a stretching sheet," Journal of the Nigerian Mathematical Society, vol. 36, no. 2, pp. 419–433, 2017.

[26] Trivedi, O. Otegbeye, M. S. Ansari, and T. Fayaz, "Flow of Jeffrey fluid near impulsively moving plate with nanoparticle and activation energy," International Journal of Thermofluids, vol. 18, Art. no. 100354, 2023, https://doi.org/10.1016/j.ijft.2023.100354.

[27] P. Ubale Patil, V. B. Kulkarni, and R. M. Lahurikar, "Effect of mass transfer and heat sources on the rotatory flow past an accelerated infinite vertical plate through a porous medium," International Journal of Intelligent Systems and Applications in Engineering, vol. 12, pp. 598–608, 2024.

[28] Vijaya Kumar and S. V. K. Varma, "Thermal diffusion and radiation effects on unsteady MHD flow past an impulsively started exponentially accelerated vertical plate with variable temperature and variable mass diffusion," International Journal of Applied Mathematics Analysis and Applications, vol. 6, no. 1, pp. 191–214, 2011.

[29] Waqas, S. A. Khan, T. Muhammad, and M. Syed, "Heat transfer enhancement in stagnation point flow of ferro-copper oxide/water hybrid nanofluid: A special case study," Case Studies in Thermal Engineering, vol. 28, Art. no. 101615, 2021, https://doi.org/10.1016/j.csite.2021.101615.

[30] Muthucumaraswamy, P. Ganesan,V.M. Soundalgekar, "On flow and heat transfer of a viscous incompressible fluid past an impulsively started vertical isothermal plate", International Journal of Thermal Sciences 40(3):297-302, 2001, DOI:10.1016/S1290-0729(00)01219-9.

[31] Ashish Khudaiwala, Rupesh Patel, "Performance investigation of high-powered light emitting diodes using copper and silicon-oxide based nanofluid filled heat pipe", J Ther Eng, Vol. 12, No. 1, pp. 16−28, January, 2026, DOI: 10.14744/thermal.0001055.

[32] Mehdi Amiri, Rasoul Karimi, Iman Abbaspour, Top of Form "Enhanced heat transfer with iron oxide nanofluids: SYNTHESIS and performance evaluation", J Ther Eng, Vol. 12, No. 1, pp. 88−98, January, 2026, DOI: 10.14744/thermal.0001060.